An adaptive scalloping suppression method for ScanSAR images based on the Kalman filter

Wei Yang, *member, IEEE*, JiaDong Deng, XinWei An, HongCheng Zeng, *member*, *IEEE*, ZiQian Ma, Wei Liu, *Senior Member*, *IEEE*, and Jie Chen, *Senior Member*, *IEEE*

***Abstract*—The ScanSAR mode can change the antenna angle during operation and obtain a wide swath by scanning multiple strips at one time. However, due to discontinuous working in azimuth, the scalloping effect in ScanSAR will degrade the image quality. In this paper, a novel adaptive scalloping suppression method is proposed by analyzing the complex scene as well as the scalloping distribution. First, the images of the various types of scenes are pre-processed so that the distribution of sub-images satisfies the Kalman filter conditions. Then, the problem of space-variant property is solved by performing adaptive blocking in the range direction. Finally, the Kalman filtering algorithm is introduced to process the scalloping in each sub-block separately, and the processed sub-blocks are fused to obtain the final result. The proposed method is verified by the real ScanSAR images of GF-3. Experimental results show that the proposed method is more efficient for scalloping suppression than the existing ones for both general and complex scenes, and has clear improvement for large-scale images with strong scalloping, which fully verifies the robustness and adaptability of the proposed method.**

***Index Terms* — ScanSAR, scalloping suppression, adaptive blocking, Kalman filter, Gaofen-3 satellite**

I. Introduction

SYNTHETIC Aperture Radar Scan Mode (ScanSAR) can change the angle of the antenna while working, and scan multiple strips at one time to obtain a wide swath, so it has been widely used in both military and civilian fields [1]. In the ScanSAR mode, wide-range imaging is realized by periodically switching the antenna beam to sub-bands of different ranges. In each sub-band, due to influence of the azimuth antenna pattern (AAP), targets located at different azimuth will have different amplitude weights, resulting in periodic azimuth amplitude modulation, which makes the ScanSAR images exhibit light and dark stripes, the so-called scalloping noise [2-4]. This noise greatly degrades the image quality, increases the difficulty of image interpretation and affects the subsequent application of the image, so scalloping suppression has become an important part of ScanSAR image processing.

The most common scalloping suppression technique is to correct this periodic variation directly on echo data by evaluating and compensating the antenna pattern during image focusing. In 1995, Bamler removed the scalloping effect by constructing a function related to azimuth, which can accurately compensate for the periodic fluctuations of ScanSAR echo intensity in azimuth [5]. However, this method can only be applied to high SNR situations, and the antenna beam pointing error will seriously affect its performance. Afterward, Vignegon improved Bamler's method, by more accurately estimating the Doppler center position of each irradiation, and increasing the signal-to-noise ratio (SNR) of the processed images [6]. Shimada performed radiation and geometric calibration of the imaging satellite by using the Amazon rainforest, accurately calculated the ScanSAR satellite's pattern, and on this basis, carried out more accurate energy fluctuation correction [7-9]. However, the above methods all require prior information of the radar sensor In addition, some researchers also improved the hardware to avoid the scalloping effect problem. By turning the azimuth antenna beam from the back to the front along azimuth during the entire acquisition process, the terrain observation by the progressive scans (TOPS) mode is developed to eliminate the scalloping effect [10], but the focus operation of sensors and imagers that implement the TOPS mode is more complicated.

In recent years, several image-based methods have been discussed and proposed. The adaptive filter proposed by Romeiser calibrates the scalloping effect by identifying the peak associated with scalloping in the image spectrum, and finds the Doppler center through multiple iterations and gradually corrects energy fluctuations [11]. This method has

This work was supported in part by the National Natural Science Foundation of China (NNSFC) under Grant No. 62101014 and No. 62271028. (Corresponding author: *HongCheng Zeng*.)

Wei Yang, JiaDong Deng, XinWei An, HongCheng Zeng, ZiQian Ma and Jie Chen are with the School of Electronic and Information Engineering, Beihang University, Beijing 100191, China (e-mail: yangweigigi@sina.com; djdong0725@buaa.edu.cn; anxinwei@buaa.edu.cn; maziqian1999@126.com; chenjie@buaa.edu.cn).

Wei Liu is with the School of Electronic Engineering and Computer Science, Queen Mary University of London, London E1 4NS, UK (e-mail: w.liu@qmul.ac.uk)

good simulation results, but the iterative process leads to a high-computational complexity, and no experimental result based on real ScanSAR data is provided. A. Sorrentino [12] extended the idea to the frequency domain and separated ScanSAR fringe information through wavelet transform. However, frequency processing cannot guarantee that the removed frequency band does not contain useful scene information, such as edges and slopes. Knut transformed the image to the frequency domain and introduced an edge detection factor to ensure useful edge information can be preserved [13]. In [14], a method based on the Kalman filter was proposed, which achieves a good de-striping effect in both simulation and real data experiments. It utilizes two parameters, gain and offset, which are periodic in azimuth, to model the sector structure. Assuming that the gain and offset parameters are constant in a certain azimuth direction, the minimum mean square error estimates for both parameters can be obtained with iterative processing through the Kalman filter by considering all samples in a certain azimuth direction as observations. According to the established scalloping fringe model, the scalloping effect in the ScanSAR image can be removed by substituting the gain and offset. However, due to the linearity and Gaussian requirements of the Kalman filter, validity of this method is based on the assumption that the brightness of the radar illuminated scene satisfies the Gaussian distribution, but the amplitude of the SAR image usually follows the Rayleigh distribution, which cannot obtain correct results in non-stationary scenes. Based on the above method, an additive noise model was proposed in [15], and image segmentation and pixel value filling was introduced for the sea-land connected scene to make the distribution of sub-images meet the requirement of Kalman filter. However, the threshold for the image segmentation and pixel filling scheme is empirical, leading to failure in some complex scenes. To overcome the shortcomings of the above method, a genetic algorithm was employed in [16] based on the maximum inter-class variance to obtain the optimal threshold for image segmentation, and further divide the image into two sub-images with different brightness. The missing pixels of each sub-image are filled with random numbers following the Gaussian distribution to provide a linear Gaussian condition for the Kalman filter. However, estimation of the threshold and brightness filling parameters cannot be achieved in a reliable way, leading to a less robust algorithm.

In this paper, a novel adaptive scalloping suppression method is proposed. First, a preprocessing operation is applied on the image to obtain a sub-image that matches the Gaussian distribution as closely as possible. Then, a clustering algorithm is proposed for adaptive blocking of sub-images in the range direction according to the distribution of scalloping intensity in the range, which can effectively reduce the effect of space-variant property. Finally, the Kalman filtering algorithm is introduced to process the scalloping in each sub-block separately, and all the processed sub-blocks are fused to obtain the final result. In addition, multiple ScanSAR images from GF-3 are selected to evaluate the proposed method, and the results show that the proposed method is robust and flexible, and has an effective performance for all kinds of scenes, and the improvement is even better for large-scale images.

The remaining parts of this paper are organized as follows. In Section II, the space-variant properties of scalloping and the problem of residual scalloping in complex scenes are analyzed, and the proposed method is presented in detail. Experimental results are provided in Section III, and conclusions are drawn in Section IV.

II. Methodology

A. Scalloping Suppression Model

In ScanSAR mode, the antenna's pointing is changed to scan multiple subswaths. Starting from the start subswath, after scanning the current subswath within a burst, the antenna changes its attitude to scan the next subswath, and after scanning multiple subswaths, it returns to the start subswath to start the next scanning cycle, as shown in Fig. 1.

The transfer function of the ScanSAR mode changes seriously with space and time, and its azimuth antenna pattern can be approximated by $\mathrm{sinc}^2(x)$ [17]. Targets at different azimuth positions are weighted by the different gains of the antenna pattern, causing the radiometric characteristic of the image to change along the azimuth. This is the scalloping of ScanSAR, which is represented by bright and dark stripes on the image, as shown in Fig. 2.

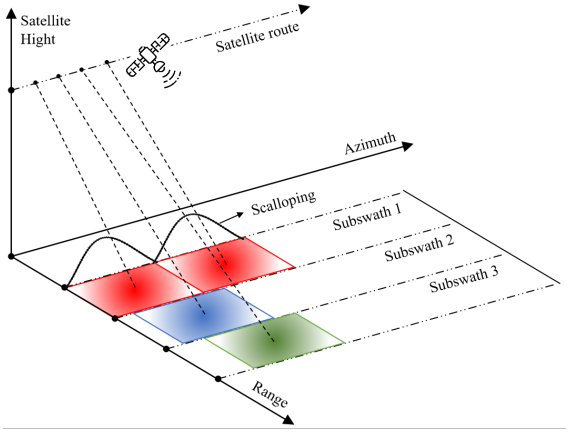

Fig. 1. ScanSAR acquisition geometry

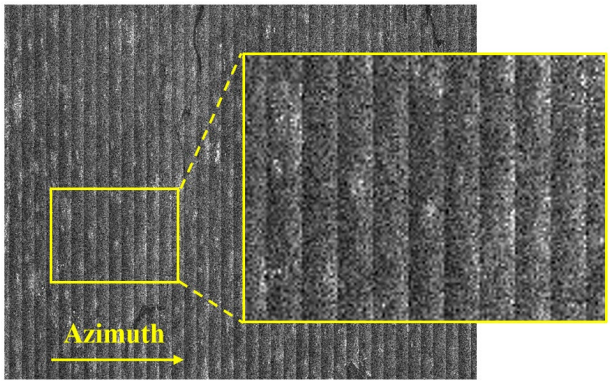

Fig. 2. Scalloping in a ScanSAR image.

Based on [15] and [16], for a noisy image with size of $m \times n$, the acquired real SAR image is regarded as the superposition of the ideal SAR image and the scalloping intensity, so the scalloping intensity estimation is modeled as

$$S_c(r,x) = S_o(r,x) + o(r,x) \quad (1)$$

where r and x represent range and azimuth respectively, S_o is the ideal image without scalloping noise, S_c is a real image containing scalloping noise, and $o(r,x)$ is the scalloping intensity of the pixel in which the range position is r and the azimuth position is x.

The intensity of scalloping in a certain azimuth can be regarded as a constant value at all range positions and then equation (1) can be simplified as

$$S_c(r,x) = S_o(r,x) + o(x) \quad (2)$$

The Kalman filter is constructed according to [16]. The prediction equation as

$$\hat{x}_k^- = \hat{x}_{k-1}^- \quad (3)$$

$$P_k^- = P_{k-1} + Q \quad (4)$$

where $\hat{x}_k^-$ is the *k*-th prior estimate, P_k^- is the prior estimation error covariance, and Q is the system noise variance.

The update equation is

$$K_k = \frac{P_k^-}{P_k^- + R} \quad (5)$$

$$\hat{x}_k = \hat{x}_k^- + K_k(z_k + \hat{x}_k^-) \quad (6)$$

$$P_k = (I - K_k)P_k^- \quad (7)$$

where K_k is the Kalman gain, $\hat{x}_k$ is the *k*-th posterior estimation, i.e., the filtering result of each step estimation, P_k is the posterior error covariance, R is the observed noise variance, and z_k is the observed value.

Based on the above model, each azimuth dimension of the processed image is filtered. For current azimuth, all range pixels are used as the observation value to perform iteration, and the filtering result of the last iteration is retained as the estimated value of scalloping intensity. Then, the result of scalloping suppression can be obtained through equation (2).

B. Filter Window and Scalloping Period

The core idea of using Kalman filtering is that the real image is regarded as noise conforming to a Gaussian distribution, and the current scalloping noise in the azimuth is regarded as a stable actual output value. Due to the influence of the scalloping noise, the current azimuth observation z_k and the noise variance *R* can not be obtained directly, and a filter window is needed.

The scalloping noise could be considered periodically distributed in the azimuth direction, and we define the number of pixel points in a cycle as a scalloping period. During a cycle, the pixel values of the real image are affected to varying degrees, either increasing or decreasing. It is possible to indirectly obtain the stabilized noise variance *R*, as well as the observed values z_k, by using a filter window of multiples of the length of the entire cycle. The noise variance *R* is taken as the variance of all pixel points within the current window. It is worth noting that only when the window length is an integer multiple of the scalloping period can *R* maintain a stable value. At the azimuth coordinate point *x*, the observation z_k has the coordinates *z(k,x)* in the image with the following equation:

$$z(k,x) = S_c(k,x) - \frac{1}{m \times (2t+1)} \sum_{i=1}^{m} \sum_{x-t}^{x+t} S_c(i,j) \quad (8)$$

where *m* is the number of pixel points of the image in the distance upward and *t* is the number of pixel points corresponding to the scalloping period, which is equivalent to T_S in equation (9).

In this paper, the length of the filter window is two scalloping periods, and the row to be read in a certain azimuth resides in the center, as shown in Fig. 3. Corresponding to equation (8), it is equal to one scalloping period. The filter window is indicated by a purple wireframe, and the row to be read is indicated by red line.

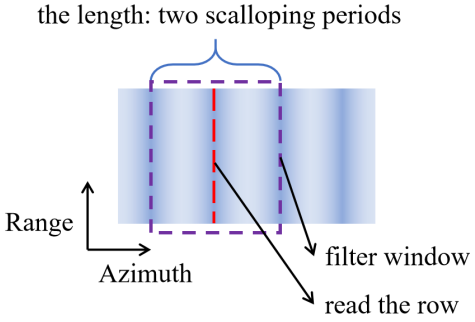

Fig. 3. Schematic of the filter window (Red line represents the row to be read and purple wireframe represents the filter window).

Considering the periodic distribution of scalloping noise in the azimuth direction, this paper chooses FFT (Fast Fourier Transform) to calculate the scalloping period. Firstly, the grayscale average value is taken in the range direction, and then the Fourier transform is carried out to find the peak point in the restricted region in the frequency domain. Finally, the accurate scalloping period can be obtained according to the following relationship:

$$T_s = \frac{1}{F_s} \quad (9)$$

where F_s is the horizontal coordinate of the peak point and T_s is the scalloping period.

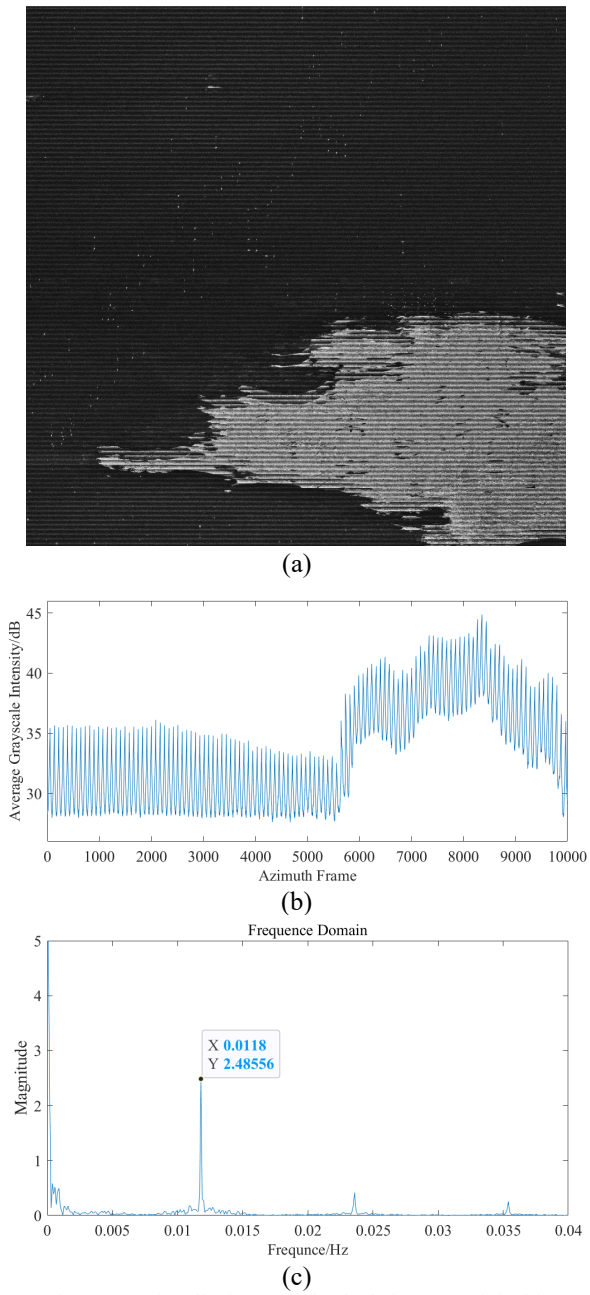

Fig. 4. Performance of scalloping period calculation: (a) original image with vertical direction as azimuth direction; (b) average grayscale intensity(AGI) of image along azimuth; (c) frequency domain performance of AGI.

As shown in Fig. 4, the image belongs to the sea-land connected scene, and the actual scalloping period is 85-pixel points. The average grayscale distribution along the azimuth can be observed that there is a clear peak period cycle. In the frequency domain, it can be seen that the horizontal coordinate of the highest peak is 0.0118, and the calculated scalloping period is 84.74, the reciprocal of 0.0118, which is very accurate.

C. Block Processing in the Range

The energy unevenness caused by the antenna pattern weighting also exists in the ScanSAR image in the range direction, that is, the scalloping intensity along range is not strictly constant but shows a certain degree of spatial variability, which is called space-variant properties in the range. One SAR image with scalloping is shown in Fig. 5, in which the uniformly scattered area (red marked area) is obtained for grayscale statistics, and the average grayscale intensity along range is obtained as shown in Fig. 5. The gray value of the calm sea surface in the ideal noise-free image should tend to be constant, while it can be seen due to the gray superposition of the scalloping noise in the actual image, the gray value of actual images in Fig. 5 changes along the range and is not constant, which intuitively shows space-variant property in the range of scalloping.

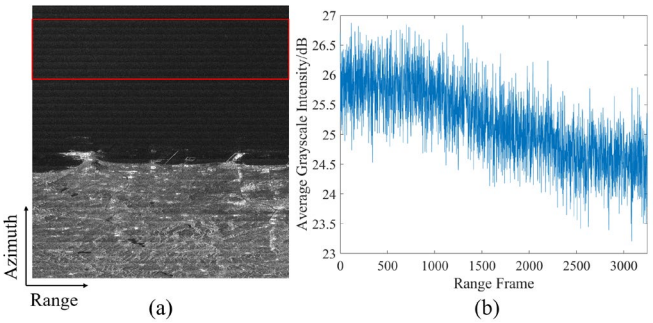

Fig. 5. The space-variant property in the range: (a) original image with vertical direction as azimuth direction; (b) the average gray intensity(AGI) of the uniformly scattered area in the range.

Based on the above-mentioned Kalman filter model, when the scalloping intensity is estimated for a certain azimuth of a scalloping noise image, only one scalloping intensity value can be obtained. Due to the influence of space-variant properties in the range, when the range is large, the actual corresponding scalloping intensities of different range gates differ greatly. Therefore, the constant scalloping intensity estimated above is not applicable to the entire range, and may introduce errors and cause scalloping to remain in some range.

The block processing scheme is proposed to solve this problem based on the above Kalman filter model in this study. When processing a specific azimuth, assuming that the spatial variability of scalloping is small within a limited range, and the error of estimating the scalloping intensity in this range as a constant value through the above Kalman filter model is within an acceptable range, thereby the constant value can be substituted into formula (2) to realize suppression of scalloping in this range. According to the above idea, in order to achieve scalloping suppression for the entire image, the image needs to be divided into blocks along range first, and filtering based on the Kalman filter is implemented for each block.

We set the local scalloping intensity function to quantitatively describe the scalloping, which performs the block processing more rigorously. Let the image with scalloping intensity be $S_c \in R(m \times n)$, where m and n denote the number of pixels in the range and azimuth directions of the image, respectively. The square of the average gray value in the range direction is given by:

$$P(j) = \left[\frac{1}{m} \sum_{i=1}^{m} S_c(i, j) \right]^2 \tag{10}$$

where i and j denote the position of the point in the range and azimuth directions. The local scalloping intensity function can be expressed as the ratio of the local maximum to the local

minimum:

$$\Delta P_{\mathrm{loc}}(j)=10\lg\left\{\frac{\max[P(j)]_{local}}{\min[P(j)]_{local}}\right\} \tag{11}$$

The mean scalloping intensity value of the image is taken as the average of a series of localized scalloping intensities:

$$\Delta P_{mean}=\frac{1}{k}\sum_{j=1}^{k}\Delta P_{\mathrm{loc}}(j) \tag{12}$$

Adaptive block processing is based on dividing the image into blocks according to the proximity of scalloping intensity in the range direction. The detailed process is given as follows:

(1) The image is uniformly divided into n blocks along the range direction, where the value of n is related to the image size and the scalloping period;

(2) Calculate the mean scalloping intensity for each block and normalize it to obtain n values;

(3) Each block selects the neighboring block with the smaller scalloping intensity difference as its own merging direction;

(4) Each block is merged sequentially according to the merging direction to obtain subimages with varying lengths in the range direction and varying intensity of scalloping.

The discussion on the average number of blocks n is as follows. Firstly, the number n should not be too small, otherwise, only 2 or 3 blocks will be obtained after merging, which is not conducive to reducing the influence of space-variant properties; Secondly, this number n should not be too large. From the calculation formula (12), it can be seen that if the number of blocks is too large, the calculation result of mean scalloping intensity is easily affected by the real image information, and the mean scalloping intensity of this block cannot be obtained. In this paper, the number n is set to 20, which is the parameter that performs well after many experiments, and the number of blocks obtained from the final merging is between 5 and 9.

(a)

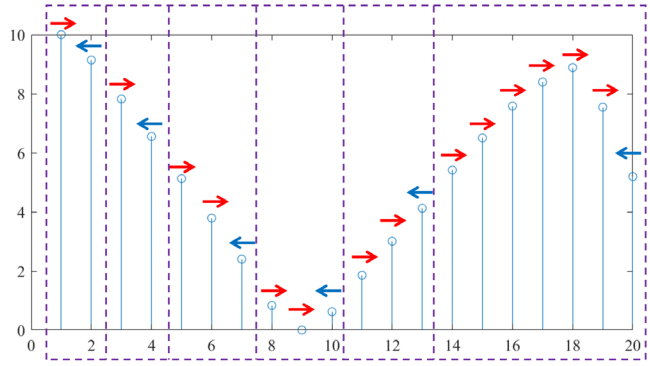

(b)

Fig. 6. Adaptive block processing in the range: (a) original image with vertical direction as azimuth direction; (b) merging of blocks (red arrows for merging to the right, blue arrows for merging to the left, and purple wireframes for adaptive merging blocks).

Fig. 6 shows the original image with the scalloping effect and the merging process. The number of pixels in the range of the original image is 10000, which is uniformly divided into 20 blocks. In Fig. 6(b), each vertical line represents the mean scalloping intensity of a sub-block, for which a merging direction is assigned, with red arrows for merging to the right and blue for merging to the left, and five sub-images of varying lengths can be merged eventually.

The processing flow is shown in Fig. 7. For a scalloping image with a size of $m \times n$, where m is the range size and n is the azimuth size, the image is divided into s blocks with unequal lengths in the range, so the size of each block is $m_s \times n$. When filtering the current block, the scalloping estimation is performed by traversing all azimuth. Take the first azimuth as an example, when estimating a specific current azimuth, the m_s pixel data corresponding to this azimuth, which is expressed as $S_c(r,1)$ in Fig. 7, is taken as the observation value, and k iterations are performed according to equations (3)-(7) to obtain estimated value of the scalloping intensity for the current azimuth, which is expressed as $o(1)$ in Fig. 7. Finally, the scalloping intensity of each image block is spliced together and smoothed along the range direction at the splices, which prevents the appearance of dividing lines at the splices. The ideal image is obtained by subtracting the scalloping intensity of the whole image from the original image.

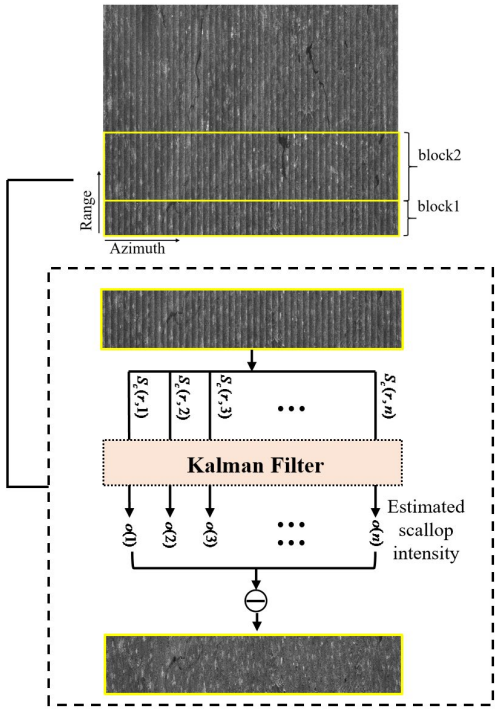

Fig. 7. Kalman filtering method based on adaptive block processing.

D. Image Segmentation Preprocessing

Sea-land connected areas usually have relatively drastic gray-scale change, which leads to instability of the Kalman filter in this area and will leave residual scalloping or even artificially introduced artifacts as shown in Fig. 8(a). At the same time, the severe grayscale change caused by the strong scattering point target in the relatively stable scene will also affect the estimation accuracy of the Kalman filter, resulting in a large scalloping residue after filtering in the azimuth with strong scattering points, as shown in Fig. 8(b). This is because the Kalman filter is suitable for Gaussian linear systems, while the SAR amplitude image follows the Rayleigh distribution. In particular, the statistical characteristics of non-stationary regions with sea-land connection and strong scatterers are quite different from the Gaussian distribution, which leads to large estimation error of the Kalman filter. Although the statistical distribution of the image does not satisfy the Gaussian distribution, the statistical distribution of each column is not much different from the Gaussian distribution, and the Kalman filter can still achieve accurate results [16]. Therefore, image segmentation preprocessing is proposed in this paper, which divides the image to be processed into multiple sub-images, so as to make the statistical characteristics of these sub-images closer to Gaussian distribution.

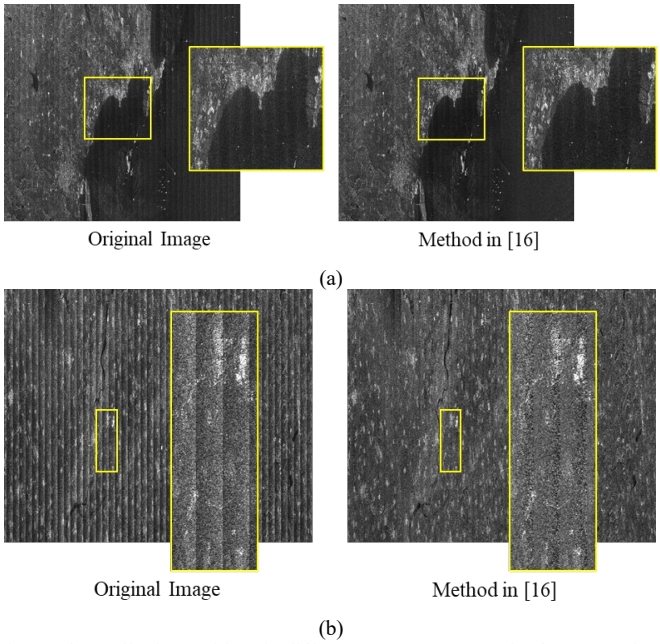

Fig. 8. The scalloping residues in different scenes: (a) a sea-land connected scene; (b) a relatively stable scene.

This solution performs different image segmentation for image scene types. The relatively stable scene containing scattering point targets will be segmented into a sub-image with strong scattering point targets and a stationary scene sub-image, and the complex scenes with sea-land will be segmented into a sea sub-image, a land sub-image and a strong scattering point sub-image.

By shielding the interference of the strong scattering points, the drastic change in gray level is avoided, so that the statistical characteristics of the stationary sub-image will be close to the Gaussian distribution; by dividing the sea and land areas, each sub-image does not have the sea-land connected area with obvious brightness difference, further avoiding the instability caused by the drastic change of gray level, and providing statistical characteristics closer to Gaussian distribution. Therefore, the stationary sub-images, sea sub-image and land sub-image obtained by the pre-processed segmentation scheme will better meet application conditions of the Kalman filter, and achieve more effective scalloping suppression.

The specific segmentation process is given as follows:

1) Strong scattering point segmentation

For non-stationary scenes, the strong scattering points cause the pixel points to deviate severely from the Gaussian distribution, leading to reduced processing effectiveness of the Kalman filter, so these points need to be extracted. In general, the number of these strong scattering points is relatively small, so by extracting the n points in each azimuth that deviate most from the mean, the image can be separated into sub-image 1 containing strong scattering points and sub-image 2.

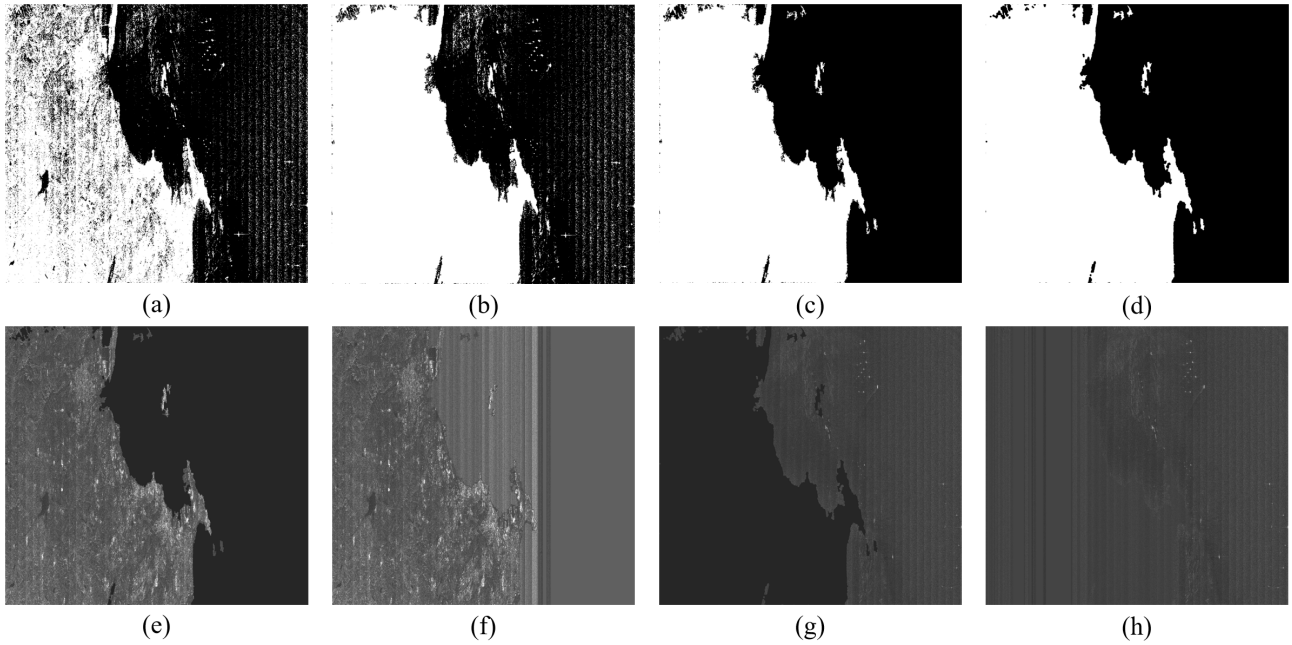

Fig. 9. Morphological segmentation of sea-land connected scene for Fig. 7(a): (a) image binarization; (b) hole filling; (c) delete small-area objects; (d) closing operation; (e) land original sub-image; (f) land filled sub-image; (g) sea original sub-image; (h) sea filled sub-image.

2) Morphological segmentation

If the scene is a sea-land connected area, the morphological segmentation process is performed on sub-image 2, and the process produces each image as shown in Fig. 9. The horizontal direction of SAR image is azimuth direction. The specific steps for morphological segmentation are as follows:

Step 1: Perform image binarization based on the gray difference between sea and land to obtain a rough segmentation. The threshold for binarization is determined automatically by the OTSU method [18] .

Step 2: On the basis of the binarized image, perform hole filling operation to fill the missing parts of the land area.

Step 3: Delete small-area objects to remove undesirable interference areas.

Step 4: Perform the closing operation to achieve spatial continuity and regional integrity of the segmented image, thereby obtaining a smooth boundary and further ensure respective connectivity of the sea area and the land area;

Step 5: Obtain the sea original sub-image and the land original sub-image based on the binary image from step 4.

Step 6: Fill in the null values. According to the mean and variance of the non-zero values of the current azimuth, fill Gaussian random numbers at all zero-valued points to make the data more consistent with the Gaussian distribution, and the detailed effect will be shown in Part 3. Obtain the ocean filled sub-image and land filled sub-image.

The statistical characteristics of the stable sub-image 2, or sea filled sub-image and land filled sub-image obtained by the segmentation method will be closer to the Gaussian distribution, thereby better satisfying the application conditions of the Kalman filter and achieving more accurate scalloping suppression. The effectiveness of this method will be analyzed and verified in the experimental part.

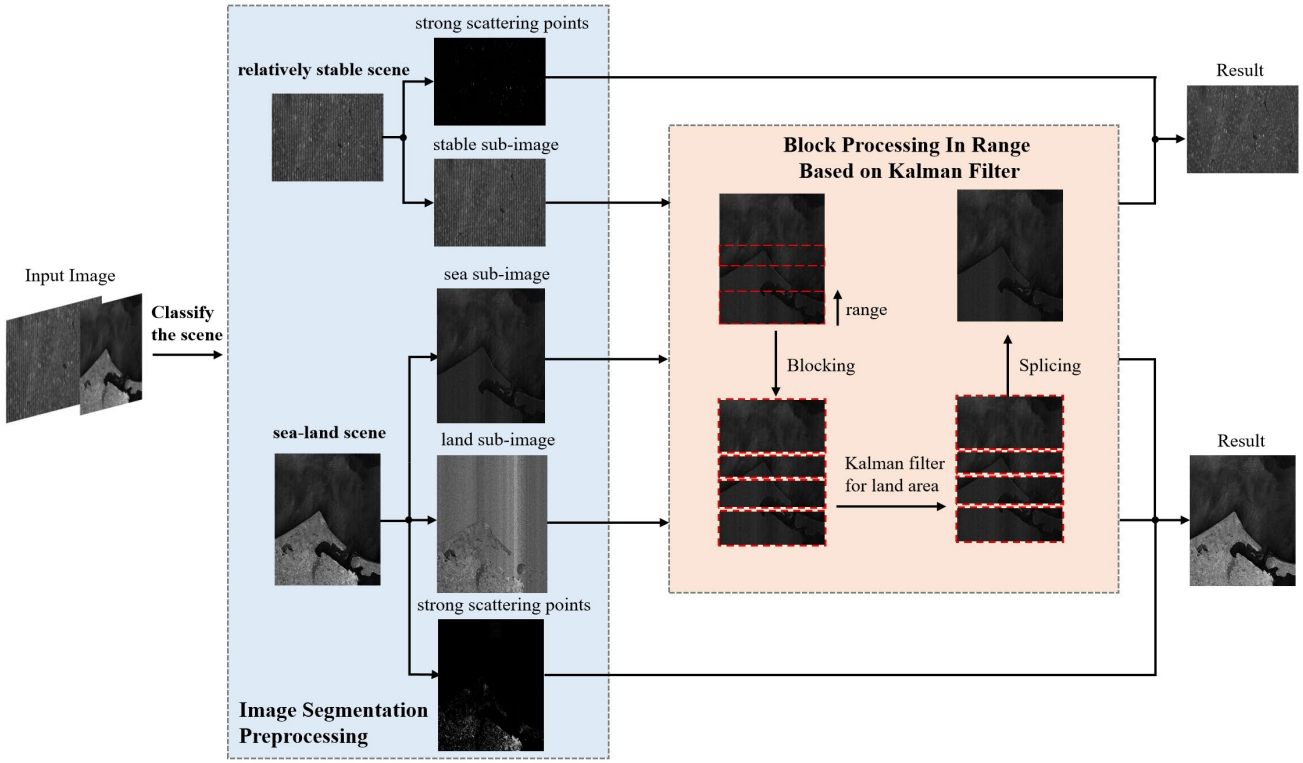

Fig. 10. Flow chart of the proposed scalloping suppression method.

E. The Proposed Method

Based on the above two improvements, the processing flow of this method is shown in Fig. 10.

For the ScanSAR image to be processed, first determine whether it is a relatively stable scene or a sea-land connected scene. After this, the image segmentation preprocessing scheme is applied to obtain the corresponding sub-images, and then Kalman filtering combined with block processing in the range is performed on the sub-images to achieve scalloping suppression, finally the sub-images are merged to obtain the final filtering result.

For the segmentation of a relatively stationary scene, it is segmented into strong scattering point sub-image and stationary sub-image, and only the stationary sub-image will be subjected to subsequent filtering processing. The sea-land connected scene is divided into sea sub-image, land sub-image and strong scattering point sub-image, and the sea sub-image and land sub-image will be filtered.

In Fig. 10, block processing in the range takes a sea sub-image as an example. First, perform division along range to obtain multiple image sub-blocks, and secondly, realize scalloping suppression for each sub-block image based on Kalman filtering.

When filtering a sub-block image, even though all pixels are involved in the filtering operation, the filled pixels do not actually affect the image negatively because the stitching operation replaces these pixels with those from the original image.

III. EXPERMENTS

In this section, GF-3 data is used to verify the effectiveness of the proposed method. First, experiments that verify the effectiveness of image segmentation are carried out. Then, the proposed method is applied to GF-3 ScanSAR images for scalloping suppression.

A. Effectiveness of Image Segmentation Preprocessing

The Jarque-Bera test can be used to measure the conformity between the image distribution and the Gaussian distribution [16], and when the J-B value is less than 2.5, the scalloping estimation error can be restricted within the allowable range, and the Kalman filter can be directly used to filter the image. Therefore, in this section, the J-B value of the sub-images obtained by segmentation will be calculated to verify the effectiveness of the image segmentation method.

(a) (b) (c)

Fig. 11. Threshold segmentation result of relatively stationary scene with horizontal direction as azimuth direction: (a) original image; (b) sub-image 1 with strong scattering points; (c) sub-image 2 without strong scattering points.

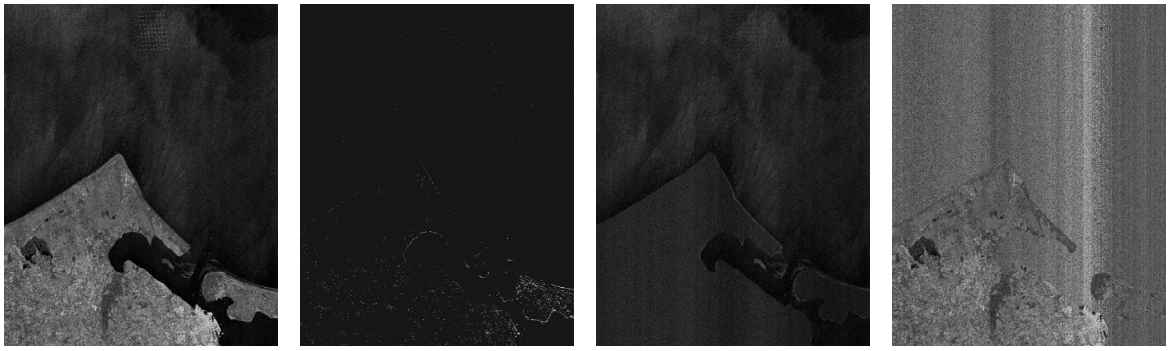

(a) (b) (c) (d)

Fig. 12. Image segmentation result of sea-land connected scene with horizontal direction as azimuth direction: (a) original image; (b) sub-image 1 with strong scattering points; (c) sea sub-image; (d) land sub-image.

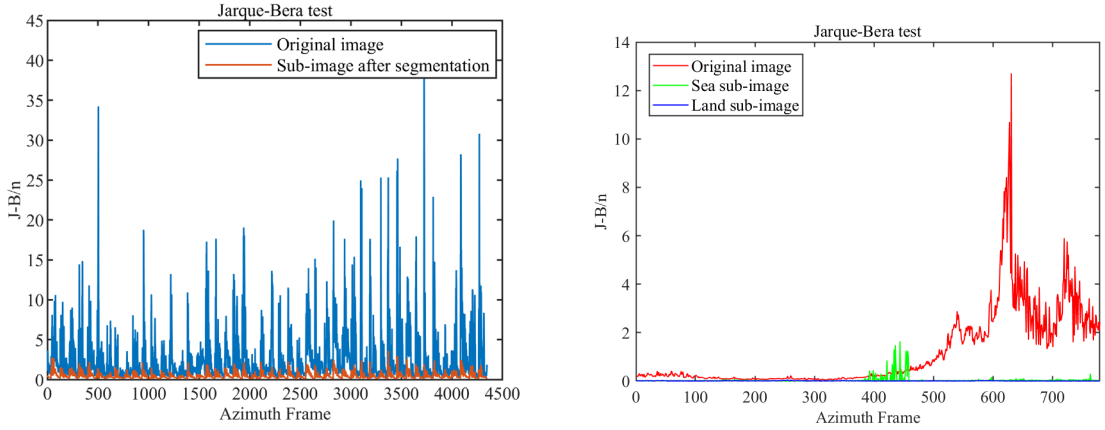

(a) (b)

Fig. 13. (a) JB parameter statistics of Fig. 10; (b) JB parameter statistics of Fig. 11.

At first, the influence of the strong scatter points on the JB parameter is studied. Figs. 11(a)-(c) show the original scene image with scalloping, sub-image 1 with strong scattering points and the sub-image 2 without strong scattering points, respectively. The J-B parameter is calculated for each azimuth of the original image and sub-image 2, as shown in Fig. 13(a). The blue curve is the J-B parameter of the original image along azimuth, and red curve is that of sub-image 2. It can be seen that the J-B parameter of sub-image 2 is greatly reduced compared with the original image, and is less than 2.5 in each azimuth, which indicates the statistical characteristics of sub-image 2 in each azimuth are closer to Gaussian distribution and can meet the application conditions of Kalman filter.

Secondly, the sea-land connected scene is segmented into a strong scattering point image, a sea sub-image and a land sub-image, as shown in Figs. 12(a)-(d). The J-B parameters are calculated for the original image, sea sub-image and land sub-image, respectively, as shown in Fig. 13(b). It can be seen that the J-B parameters of each azimuth of the two sub-images are lower than 2.5, which is closer to the application conditions of Kalman filter.

Therefore, both have shown that the proposed image segmentation preprocessing step can effectively generate a result closer to Gaussian distribution as desired.

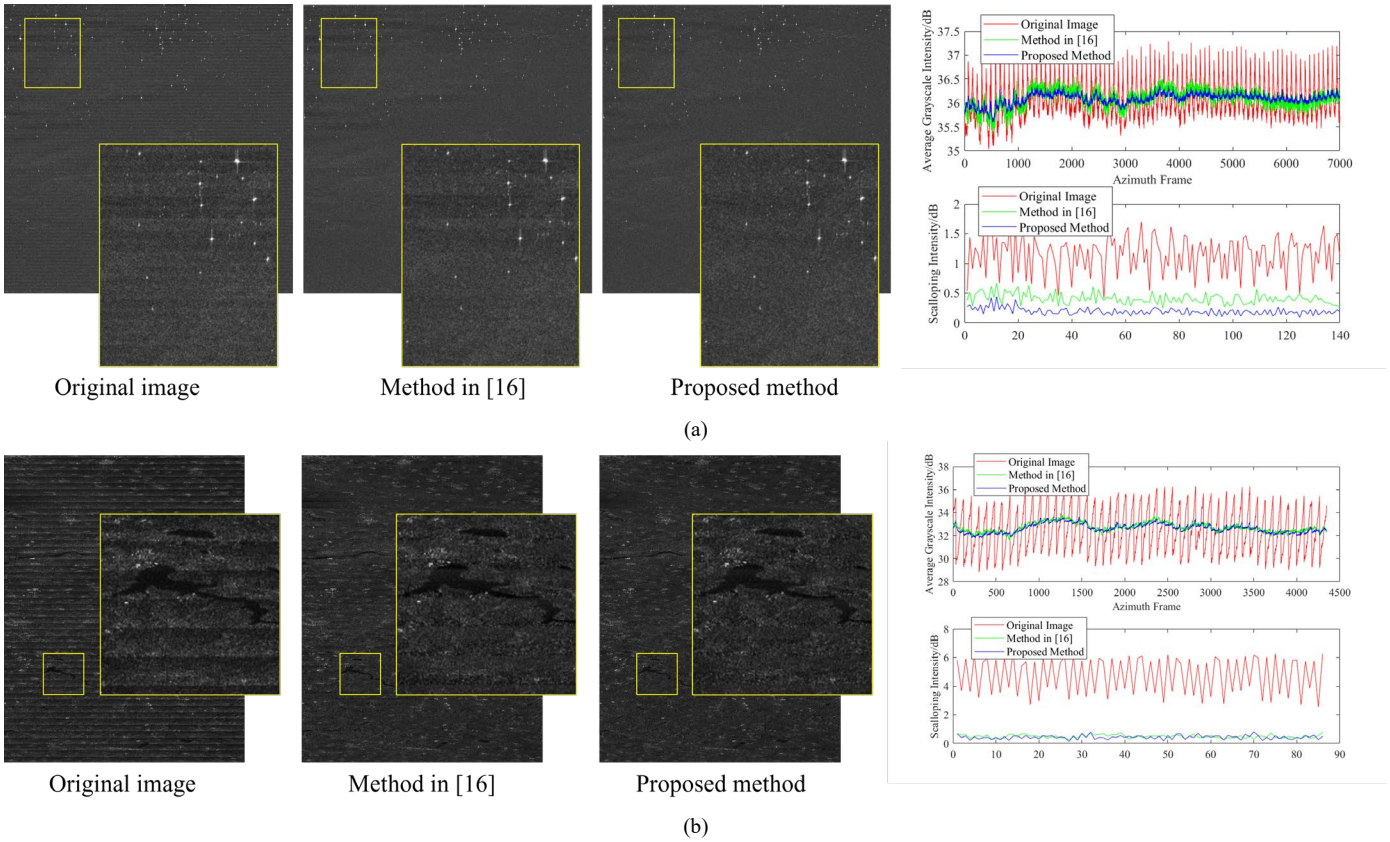

Fig. 14. Scalloping suppression results for relatively stable scenes with vertical direction as azimuth direction: (a) sea scene; (b) land scene.

B. Scalloping Suppression Results

In order to quantify the effect of scalloping suppression by the proposed method, the average gray intensity index is introduced, which is defined as the average grayscale of a column in the tested area [16], given below

$$AGI(a) = 20 \cdot \log\left[\frac{\sum_{i=1}^{r} I(a,i)}{r}\right] \tag{13}$$

1) Processing results of relatively stable scenes

Fig. 14(a) shows the processing result of a stable ocean scene. There is still obvious scalloping residue after the processing by the method in [16], but after processing by the proposed method, there is almost no scalloping residue visually, and the texture of the ocean scene is clearly visible. In order to quantitatively compare the scalloping intensity of the original image and the processed image, we use AGI and local scalloping intensity to represent and draw them in a graph. As shown in Fig. 14(a), the sharp fluctuation of the red curve reflects the light and dark scalloping noise in the original image. The green curve and the blue curve are the results after processing by the method of [16] and our proposed one, respectively. Compared with the curves of the original images, both methods have significantly reduced scalloping and smoothed fluctuations in the red curve, but the blue curve can be seen to perform better. Therefore, the scalloping in the image has been effectively suppressed by the proposed method.

Fig. 14(b) is a relatively stable land image with strong scattering points. It is divided into strong scattering point areas and stationary sub-images, and the stationary sub-image is filtered by the Kalman filter. From Fig. 14(b), in the result of the method in [16], it can be seen that scalloping in most areas is effectively suppressed, but due to the influence of spatial variation in the range, there are obvious scalloping residues in some areas. In the result of the proposed method, scalloping in all regions is well suppressed, and details of the river are preserved. At the same time, it can also be seen from the average grayscale curve that the fluctuation trend of the blue curve (processing result by the proposed method) is more in line with the red curve of the original image than the green curve (result by the method in [16]).

Clearly, the method proposed in this work can effectively suppress scalloping in relatively stable scenes, while maintaining sufficient details.

2) Processing results of sea-land connected scenes

The sea-land scenes of GF-3 images working in scanning mode are used as experimental data in this part.

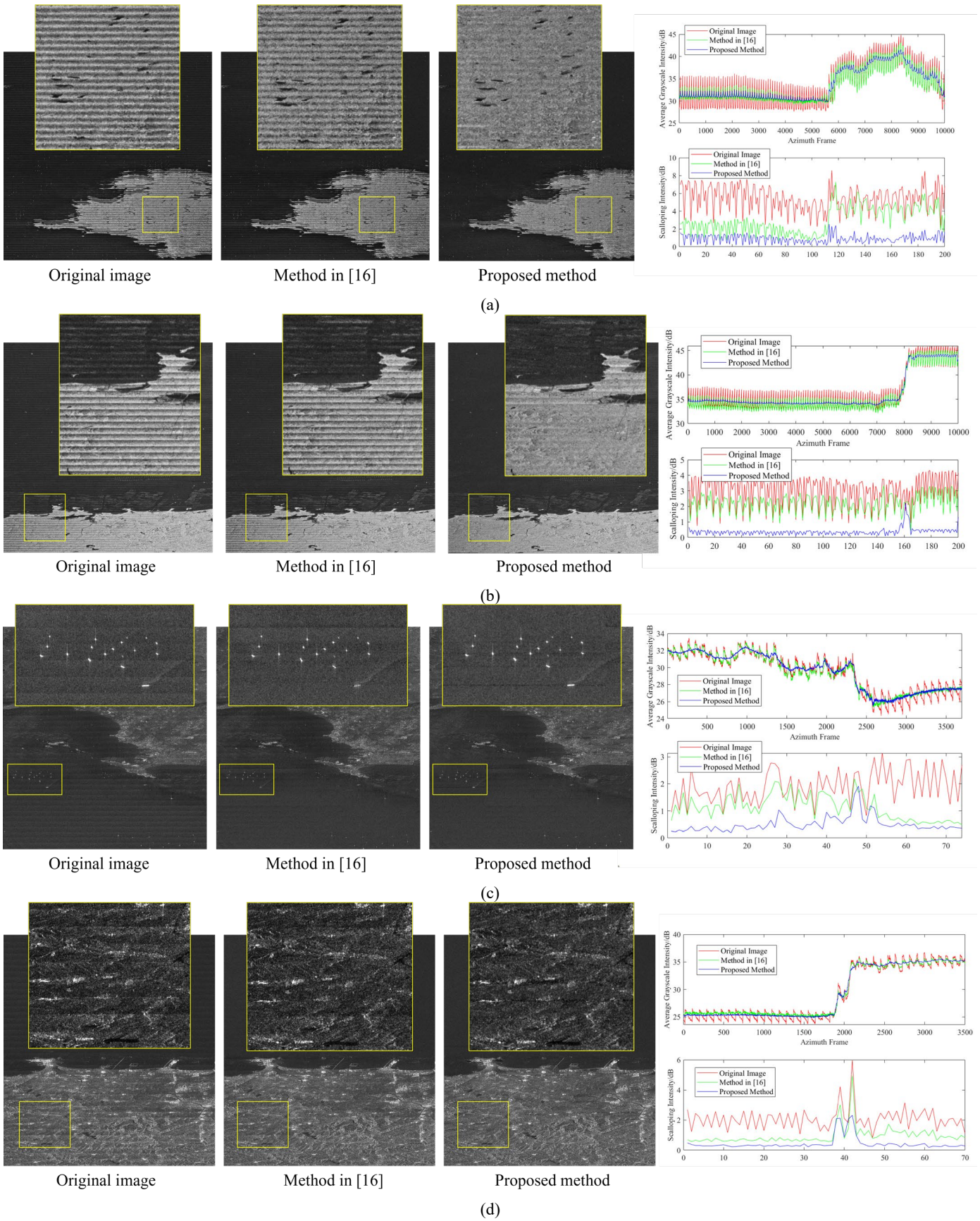

Fig. 15. Scalloping suppression results for sea-land connected scenes with vertical direction as azimuth direction: (a) and (b) are large-scale images with strong scalloping; (c) and (d) are small-scale images with weak scalloping.

Fig. 15(a) shows a sea-land connected scene in the GF-3 scan mode. It can be seen that the original image has a serious scalloping problem. After processing by the method in [16], there are still obvious scalloping effect in the land area. With the average gray level of the curves, it can be observed that scalloping is indeed suppressed to a certain extent in the ocean part, but the improvement is very limited in the land part due to the effect of the residual shadow, which is also supported by the local scalloping intensity curves. In contrast, the blue line consistently maintains a very low value during the process in the local scalloping intensity image, indicating that the proposed method has further suppressed the scalloping compared with the method in [16].

Fig. 15(b) shows the before and after image processing results with scalloping noise. It is a scene dominated by ocean areas and connected with the land. In the observation of the land area, we can find that the distribution of scalloping intensity is completely uneven in the azimuth frame, and there is almost no scalloping noise visually on the far right. In the land area, the suppression effect by the method in [16] is almost non-existent, but the disappearance of scalloping can be clearly observed in the result obtained by the proposed method. Through observation of the local scalloping intensity image, except for the peak caused by the land-sea interface in the middle part, it can be seen that the blue curve almost always maintains a much lower value than the green one, which means that our method is more effective in suppressing the scalloping noise in this area.

Fig.15(c) shows one group of experimental results with weak scalloping noise. The line between land and sea in the image is very irregular. In the ocean area, it can be observed that scalloping remains in the image processed by the method in [16], and the brightness of the ship is reduced. Correspondingly, the image processed by the proposed method not only has better suppression effect, but also retains the ship target well. In the average gray intensity curve, the blue curve is smoother than the green one, that is, the proposed method can also perform well in the scene with weak scalloping noise, which further verifies the effectiveness of the proposed method.

Fig. 15(d) shows another GF-3 scan mode scene with weak scalloping noise. The overall brightness of the image is relatively low, and the boundary line between sea and land is basically parallel to the range frame. From the average gray curve, the change of the blue curve is always more gentle than that of the green curve, and the same is true from the local scalloping intensity curve, which further supports the effectiveness of the proposed method.

C. Effectiveness of Block Processing in the Range

The necessity and effectiveness of block processing in the range is further discussed in this section. Two scenes were chosen for the experiments: the sea-land connected scene and the relatively stable scene.

For the sea-land connected scene, Fig. 15(b) was selected for analysis, as shown in Fig. 16, where (a) is the filtering result with only image segmentation preprocessing but without block processing, and (b) is the filtering result by the proposed method. The vertical direction of SAR image is azimuth direction. Two regions are selected from the land area and the sea area for comparative analysis. It can be seen that there is still serious scalloping noise in the two areas of (a), but the scalloping noise in (b) has been significantly suppressed. The blue region is quantitatively analyzed, and the grey intensity graph is drawn along azimuth as shown in (c), where the red curve is the performance of scalloping in the original image, and the green curve and the blue curve correspond to (a) and (b), respectively. The level of the green curve is significantly lower than the level of the red curve; in other words, the brightness of the image is reduced, which is undesirable. Intuitively, the fluctuation of the blue curve is lower than that of the green curve, which further demonstrates that there is less scalloping remaining in (b). As a result, we can say that block processing in the range can effectively solve the problem caused by the space-variant properties in the range.

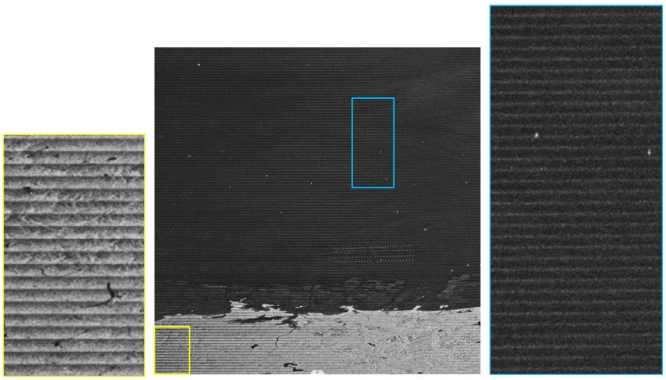

(a)

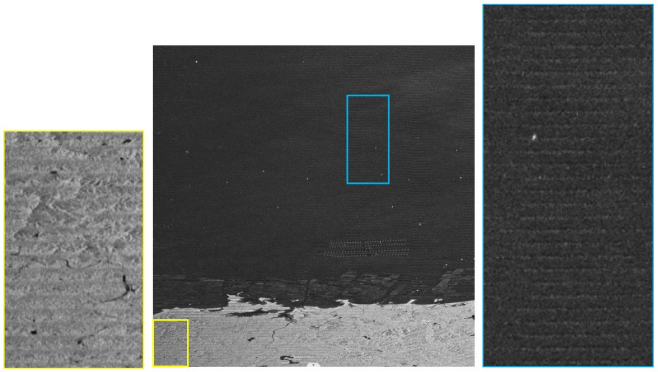

(b)

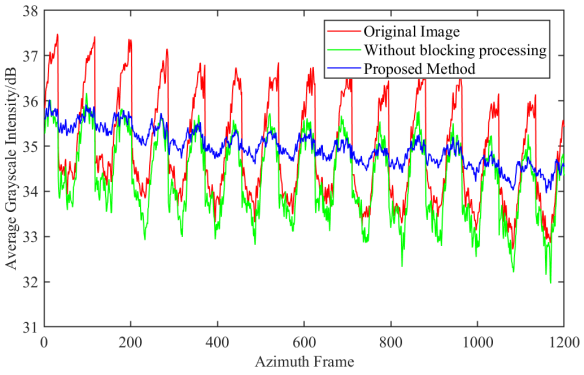

(c)

Fig. 16. Effectiveness of block processing in the range of sea-land connected scene: (a) result without block processing in the range; (b) result of the

proposed method; (c) comparison of average grey intensity curve.

For the relatively stable scene, Fig. 14(b) was selected for analysis, as shown in Fig. 17, where both the yellow region and the blue region in (a) have obvious scalloping noise, while the corresponding regions in (b) have almost no scalloping. The horizontal direction of SAR image is azimuth direction. The yellow region is further selected to calculate the average gray intensity curve along azimuth, and the degree of fluctuation of the green curve is much lower than that of the blue one.

In summary, both visual and quantitative analysis have verified the necessity and effectiveness of the proposed block processing in the range.

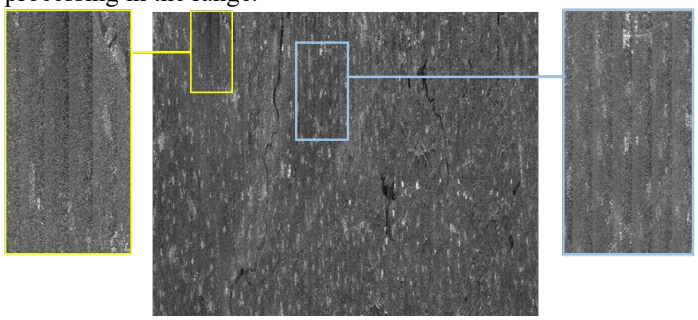

(a)

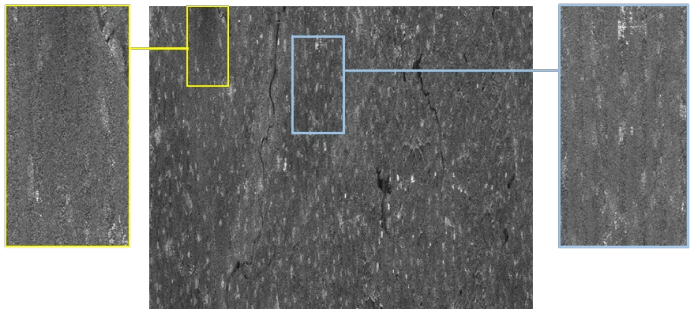

(b)

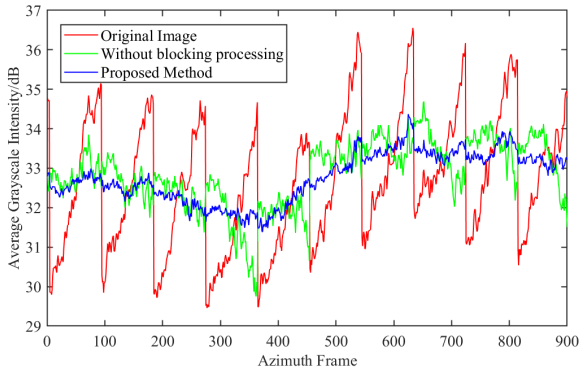

(c)

Fig. 17. Effectiveness of block processing in the range of relatively stable scene: (a) result without block processing in the range; (b) result of the proposed method; (c) comparison of the average grey intensity curve.

D. The Mean Scalloping Intensity Index

The above experimental results use the mean scalloping intensity by equation(12) for quantitative evaluation, which can measure the degree of scalloping residue in the whole image, and the results are shown in Table 1.

As can be seen, the proposed method further reduces the scalloping compared to the method in [16]. Among them, the average scalloping intensity from Fig. 15(a) and Fig. 15(b) has the largest reduction, which is due to the larger image size (10000×10000 pixel dots) and the more severe space-variant properties in the range. In other words, the proposed method has a better performance for images with a larger size.

TABLE I
THE MEAN SCALLOPING INTENSITY OF THE IMAGES

	Original	Method in [16]	Proposed method
Fig. 10(a)	1.15dB	0.36dB	0.17dB
Fig. 10(b)	4.78dB	0.43dB	0.35dB
Fig. 11(a)	5.41dB	2.81dB	0.38dB
Fig. 11(b)	3.03dB	2.15dB	0.21dB
Fig. 11(c)	1.90dB	1.02dB	0.41dB
Fig. 11(d)	2.08dB	0.79dB	0.31dB

IV. CONCLUSION

The space-variant properties of scalloping in the range and the residual scalloping in the complex scenes have been analyzed, and a robust method for scalloping suppression for various scenes has been proposed, including the block processing scheme in the range and the image segmentation preprocessing stage, which greatly improves the scalloping suppression performance. The experiments results based on GF-3 ScanSAR images show the proposed method can effectively deal with the problem of space-variant properties in the range and has a good performance in sea-land connected scenes. At the same time, good adaptability has been achieved by the proposed method, which is mainly reflected in three aspects: 1) for ScanSAR images with different complexity, the image segmentation step is adaptive and more accurate; 2) for images with different sector cycles, the selection of filter window length is adaptive; 3) for images with different sizes, the block size is adaptive. The whole scalloping suppression process does not require parameter adjustment and is easy to implement. In future research, a more robust morphological segmentation method can be considered to deal with more complex scenes.

REFERENCES

[1] H. Wang and X. Jia, “Improvement of image resolution in ScanSAR simulation”, in 3rd CISP, Yantai, China, Oct. 2010.
[2] S. Wollatadt et al., “Scalloping correction in TOPS imaging mode SAR data”, IEEE Geosci. Remote Sens. Lett., vol. 9, no. 4, pp. 614-618, Jul. 2012.
[3] M. Shimada. “A new method for correcting ScanSAR scalloping using forests and inter-Scan banding employing dynamic filtering”, IEEE Trans. Geosci. Remote Sens., vol. 47, no. 12, pp. 3933 – 3942, Sep. 2009.

[4] N. Li, et al., “Processing sliding mosaic mode data with modified full-aperture imaging algorithm integrating scalloping correction”, IEEE J-STARS, Vol. 10, no. 5, pp. 1804-181, May. 2017.
[5] R. Bamler, “Optimum look weighting for burst-mode and ScanSAR processing”, IEEE Trans. Geosci. Remote Sens., vol.33, no. 3, pp. 722-725, May. 1995.
[6] VIGNERON C M. Radiometric image quality improvement of scansar data[D]. Ottawa：Carleton University，2001.
[7] M. Shimada, “Long-term stability of L-band normalized radar cross section of Amazon rainforest using the JERS-1 SAR”, Canadian J. of Remote Sensing, vol. 31, no. 1, pp. 132-137, 2005.
[8] M. Shimada et al., “PALSAR radiometric and geometric calibration”, IEEE Trans. Geosci. Remote Sens., vol. 4, no. 13, pp. 3915-3932, Dec. 2009.
[9] M. Shimada. A new method for correcting scansar scalloping using forests and inter SCAN banding employing dynamic filtering[J]. IEEE Transactions on Geoscience & Remote Sensing，2009，47（12）：3933-3942.
[10] S. Wollatadt et al., “Scalloping correction in TOPS imaging mode SAR data”, IEEE Geosci. Remote Sens. Lett., vol. 9, no. 4, pp. 614-618, Jul. 2012.
[11] R. Romeiser et al., “A new scalloping filter algorithm for scansar images” in IGARSS, Honolulu, HI, USA. pp. 4079-4082, Jul. 2010.
[12] A. Sorrentino et al., “A post-processing technique for scalloping suppression over ScanSAR images”, in EUCAP, Prague, Czech Republic. pp. 2164-3342, Jun. 2012.
[13] Landmark, Knut & Solberg, Anne H Schistad (2015). Reducing scalloping in synthetic aperture radar images using a composite image transform. Proceedings of SPIE, the International Society for Optical Engineering. ISSN 0277-786X. 9643(Image and Signal Processing for Remote Sensing XXI).
[14] M. Iqbal and J. Chen, "Removal of scalloping in ScanSAR images using Kalman filter," 2012 IEEE International Geoscience and Remote Sensing Symposium, Munich, 2012, pp. 260-263, doi: 10.1109/IGARSS.2012.6351588.
[15] G. Xinwei et al., “Suppression of Scalloping and Inter-Scan Banding in Non-Stationary ScanSAR Images Based on Kalman Filter and Image Segmentation”, Journal of Naval Aeronautical and Astronautical University, vol. 132, no.5, pp. 125-129+134, Dec. 2017.
[16] W. Yang, Y. Li, W. Liu, J. Chen, C. Li and Z. Men, “Scalloping Suppression for ScanSAR Images Based on Modified Kalman Filter With Preprocessing,” in IEEE Transactions on Geoscience and Remote Sensing, vol. 59, no. 9, pp. 7535-7546, Sept. 2021, doi: 10.1109/TGRS.2020.3034098.
[17] I. G. Cumming and F. H. Wong, Digital Processing of Synthetic Aperture Radar Data Algorithms and Implementation. Norwood, MA: Artech House, 2005.
[18] Q. Chen, L. Zhao, J. Lu, G. Kuang, N. Wang, and Y. Jiang, “Modified two-dimensional Otsu image segmentation algorithm and fast realisation,” IET Image Process., vol. 6, no. 4, pp. 426–433, Jun. 2012.

Wei Yang (*Member*, *IEEE*) was born in 1983. He received the M.S. and Ph.D. degrees in signal and information processing from Beihang University (BUAA), Beijing, China, in 2008 and 2011, respectively. From 2011 to 2013, he held a post-doctoral position at the School of Electronics and Information Engineering, Beihang University. Since July 2013, he has been with the School of Electronics and Information Engineering, BUAA, as a Lecturer. From 2016 to 2017, he researched as a Visiting Researcher with the Department of Electronic and Electrical Engineering, University of Sheffield, Sheffield, U.K. He has been an Associate Professor with the School of Electronics and Information Engineering, BUAA, since 2018. He has authored or coauthored more than 60 journal and conference publications. His research interests include moving target detection, high-resolution spaceborne SAR image formation, SAR image quality improvement, and 3-D imaging.

Jiadong Deng was born in 1995. He received his B.S. degree in information and computational science from Beihang University, Beijing, China, in 2017, where he is currently pursuing his Ph.D. degree in signal and information processing. His research interests include spaceborne synthetic aperture radar (SAR) image formation for terrain observation by progressive scans (TOPS) mode and sliding spotlight mode.

XinWei An was born in 2001. He received the B.E. degree from University of Electronic Science and technology of China in 2022. He is currently pursuing the M.S. degree in signal and information processing from Beihang University (BUAA), Beijing, China. His research interests include SAR image quality improvement and SAR image interpretation.

HongCheng Zeng (*Member*, *IEEE*) was born in 1989. received the B.S. degree from China Agriculture University in 2011, the Ph. D. degree in signal and information processing from the Beihang University, Beijing, China, in 2016. Since 2019, He has been an Assistant Professor with the School of Electronics and Information Engineering, Beihang University. He was a Visiting Researcher with the School of Mathematics and Statistics, University of Sheffield, Sheffield, U.K., from 2017 to 2018. He has published more than 20 journal and conference papers, His research interests include high-resolution spaceborne SAR image formation, passive radar signal processing and moving target detection.

ZiQian Ma was born in 1999. She received the B.E. degree in Electronic Engineering from Beihang University (BUAA), Beijing, China，in 2021, where she is currently pursuing the M.S. degree in signal and information processing. Her research interests include SAR image quality improvement and SAR image interpretation.

Wei Liu (*Senior Member*, *IEEE*) received his BSc and LLB. degrees from Peking University, China, in 1996 and 1997, respectively, MPhil from the University of Hong Kong in 2001, and PhD from University of Southampton, UK, in 2003. He then worked as a postdoc first at Southampton and later at Imperial College London. In September 2005, he joined the Department of Electronic and Electrical Engineering, University of Sheffield, UK, first as a Lecturer and then a Senior Lecturer. Since September 2023, he has been a Reader at the School of Electronic Engineering and Computer Science, Queen Mary University of London, UK. He has published 390+ journal and conference papers, five book chapters, and two research monographs titled "Wideband Beamforming: Concepts and Techniques" (Wiley, March 2010) and "Low-Cost Smart Antennas" (Wiley, March 2019), respectively. His research interests cover a wide range of topics in signal processing, with a focus on sensor array signal processing and its various applications, such as robotics and autonomous systems, human computer interface, radar, sonar, and wireless communications. He is a member of the Digital Signal Processing Technical Committee of the IEEE Circuits and Systems Society (Chair from May 2022) and the Sensor Array and Multichannel Signal Processing Technical Committee of the IEEE Signal Processing Society (Chair for 2021-2022), and an IEEE Distinguished Lecturer for the Aerospace and Electronic Systems Society (2023-2024). He also acted as an associate editor for IEEE Trans. on Signal Processing, IEEE Access, and Journal of the Franklin Institute (2021-2023), and currently he is an Executive Associate Editor-in-Chief of the Frontiers of Information Technology and Electronic Engineering.

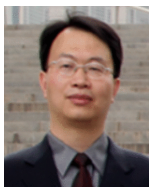

Jie Chen (*Senior Member*, *IEEE*) was born in 1973. He received the B.S. and Ph.D. degrees in information and communication engineering from Beihang University, Beijing, China, in 1996 and 2002, respectively. Since 2004, he has been an Associate Professor with the School of Electronics and Information Engineering, Beihang University. He was a Visiting Researcher with the School of Mathematics and Statistics, University of Sheffield, Sheffield, U.K., from 2009 to 2010, working on ionospheric effects on low-frequency space radars that measure forest biomass and ionospheric electron densities. Since July 2011, he has been a Professor with the School of Electronics and Information Engineering, Beihang University. His research interests include multimodal remote sensing data fusion, topside ionosphere exploration with spaceborne HF/VHF-synthetic aperture radar (SAR) systems, and high-resolution spaceborne SAR image formation and SAR image quality enhancement.